# Functional and Transcriptional Analysis of Chromosomal Encoded *hipBA*$^{Xn2}$ Type II Toxin-Antitoxin (TA) Module From *Xenorhabdus Nematophila*

**Mohit Yadav**
Gautam Buddha University
**Jitendra Rathore** ( jitendra@gbu.ac.in )
Gautam Buddha University https://orcid.org/0000-0002-2915-7824

**Research Article**

**Keywords:** Xenorhabdus nematophila. Toxin-Antitoxin. hipBA. Promoter. Overexpression. Escherichia coli

**Posted Date:** March 18th, 2021

**DOI:** https://doi.org/10.21203/rs.3.rs-306649/v1

# Abstract

*Xenorhabdus nematophila* is an entomopathogenic bacterium that synthesizes numerous toxins and kills its larval host. The genome of this bacterium also encodes a total of 39 putative toxin-antitoxin (TA) systems. These systems are also associated with maintaining the bacterial genomic stability and survival of bacteria under adverse environmental conditions. Three *hipBA* TA homologs were identified on the chromosome of *X. nematophila*, among them first *hipBA*$^{Xn}$ TA has been studied, second *hipBA*$^{Xn2}$ TA is still unexplored while third *hipBA*$^{Xn3}$ TA has been reported as a *pseudo*-type TA system. Thus, for the first time, here, we are exploring the functionality of the type II *hipBA*$^{Xn2}$ TA system. This TA system was identified in the genome of *X. nematophila* ATCC 19061 (NCBI Refseq NC_014228) at position 3774379–3775635 bp, which consists of *hipA*$^{Xn2}$ toxin gene encoding 270 amino acid residues protein and *hipB*$^{Xn2}$ encoding antitoxin of 135 amino acid residues protein. It was observed that the overexpression of HipA$^{Xn2}$ toxin inhibits the growth of *Escherichia coli* cells in a bacteriostatic manner and amino-acids G8, H164, N167, and S169 were key residues for its toxicity. Promoter activity and expression profiling of messenger RNA from the *hipBA*$^{Xn2}$ TA system was also studied and showed that it was activated in both *E. coli* as well as *X. nematophila* upon exposure to different stress conditions. Further, we have exhibited the binding features of HipA$^{Xn2}$ toxin and HipB$^{Xn2}$ antitoxin to their promoter. This study provides the first evidence for the presence of a functional and active *hipBA*$^{Xn2}$ TA system in *X. nematophila*.


# Introduction

Bacteria have a typical genetic system that is responsible for the extensive potential for survival in various adverse environments like temperature variance, nutritional starvation, antibiotics, and other unfavorable conditions (Boutte and Crosson 2013). Under such conditions, *Xenorhabdus nematophila* (*X. nematophila*) is a highly successful pathogen with an ability to kill insects (Stilwell et al. 2018).

*X. nematophila* is an entomopathogenic bacterium and symbiotic to *Steinernema carpocapsae* nematode (Park and Kim 2000). This bacterial association of nematode is very lethal to many insects and considered as the cause of death in insect larvae (Mahmood et al. 2020). At the juvenile stage, free-living, nematode *S. carpocapsae* invade through the digestive tract in the insect. Nematodes penetrate the insect larvae body chambers and liberate *X. nematophila* into the hemolymph (Martens et al. 2003). Bacteria doubles quickly and thus kill larvae by secreting toxins. By whole-genome sequencing, it was observed that *X. nematophila* is a reservoir of numerous biological molecules and have great biosynthetic potential (Bentley et al. 2002; Chaston et al. 2011). A range of regulatory proteins and alarming molecules like (p)ppGpp, poly-phosphates, sigma factors, toxin-antitoxin (TA), etc. are involved in the adaptation to various adverse environments (Manganelli et al. 2004; Gerdes and Maisonneuve 2012; Maisonneuve et al. 2013; Singh et al. 2013).

TA systems are abundantly discovered in numerous bacteria and archaea (Song and Wood 2020). These are primarily consisting of a protein toxin and an RNA or protein antitoxin component. The toxin may

suspend some essential cellular processes in a similar pattern like an antibiotic while antitoxin covers up the toxin's activity. In bacterial cell physiology, TA systems are involved in biofilm formation, phage inhibition, genetic element maintenance, persister cell formation, and growth diminution during stress (Page and Peti 2016; Song and Wood 2020). TA systems have been classified in eight different classes and among them, the type II TA system is the most investigated (Song and Wood 2020).

In our previous study, we have analyzed TAome for type II TA systems in *X. nematophila* (Yadav and Rathore 2018a) and found there were three different *hipBA* TA homolog loci present in this TAome. One homolog named as *hipBA*$^{Xn}$ was already described as a bonafide type II TA system and *hipBA*$^{Xn3}$ was a *pseudo*-type TA system (Mohit Yadav & Jitendra Singh Rathore 2020) while other *hipBA*$^{Xn2}$ TA system was still not studied. Thus, to determine that these *hipBA* homolog operons encode active TA systems, it is needed to study them. In this study, we are exploring the activity of type II *hipBA*$^{Xn2}$ TA operon on the chromosome of *X. nematophila.* We have performed the functional and transcriptional attributes of a typical type II TA system to study the activity of the *hipBA*$^{Xn2}$ TA system.

# Materials And Methods

### Bacterial Strains, primers, and culture conditions

Bacterial strains and plasmids are listed in Table S1 and primers are in Table S2. We used *X. nematophila* strain 19061 and cultured it at 28ºC with 220 rpm shaking conditions. Other strains were *E. coli* DH5$\alpha$ (Bethesda Research Laboratories) used as a cloning host, *E. coli* TOP10 cells (Invitrogen) used for toxicity assay, and *E. coli* BL21 (DE3) (Novagen) used in protein expression analysis. These strains were cultivated in Luria-Bertani (LB) medium with 220 rpm shaking conditions at 37°C. With the requirement, culture media was supplemented with 100 $\mu$g mL$^{-1}$ ampicillin and 50 $\mu$g mL$^{-1}$ kanamycin. Primers were synthesized by Integrated DNA Technologies (IDT) and other chemicals were used from HiMedia laboratories. Enzymes were purchased from New England Biolabs (NEB).

### Bioinformatics of Putative *hipBA*$^{Xn2}$ TA system

Popular web tools TAfinder (version 2.0) (http://202.120.12.133/TAfinder/index.php) and TASmania (Akarsu et al. 2019) were used to identify the *hipBA*$^{Xn2}$ TA locus on the chromosome of *X. nematophila* ATCC 19061(NCBI RefSeq NC_014228). BLASTp algorithm was used to search for homologs of TA proteins. 3-D models of HipA$^{Xn2}$ toxin and HipB$^{Xn2}$ antitoxin proteins were generated by I-TASSER sever (Zhang 2008; Roy et al. 2010; Yang et al. 2014) using the threading approach. The quality of these predicted models was assured by Ramachandran plot 2.0 software (Gopalakrishnan et al. 2007) and visualized by the molecular visualization tool PyMol (Schrödinger 2002). MAFFT (Katoh and Standley 2013) application was applied for multiple sequence alignment of HipA$^{Xn2}$ and HipB$^{Xn2}$ proteins and exhibited by ESPript 3.0. (Robert and Gouet 2014). Phylogenetic trees were built in MEGA X (Kumar et al.). Promoter analysis of the upstream region of the *hipBA*$^{Xn2}$ TA system was performed by BPROM (Solovyev and Salamov 2010).

## Cloning of *hipBA*$^{Xn2}$ TA genes

The primer sequences and recombinant constructs used in this work were listed in Table S2 and Table S1, respectively. Cloning strategy involved the primer 1 and primer 2 with *Pst*I and *Hind*III restriction enzymes sites respectively to amplify 813 bp of *hipA*$^{Xn2}$ toxin gene from the genome of *X. nematophila* by polymerase chain reaction (PCR). *ara* promoter characterized vector pBAD/His C and amplified PCR products were digested with *Pst*I and *Hind*III. These digested products were further ligated to produce a recombinant construct pJSM1. In the cloning of the *hipB*$^{Xn2}$ antitoxin gene, primer 3 and primer 4 containing *Bam*HI and *Hind*III sites respectively were used to amplify 408 bp of antitoxin gene. Expression vector pET28 (a) and amplified PCR products were digested with *Bam*HI and *Hind*III and ligated to produce a recombinant construct pJSM2. Likewise, a full *hipBA*$^{Xn2}$ TA operon of 1221 bp size, comprising the *hipB*$^{Xn2}$ antitoxin gene and *hipA*$^{Xn2}$ toxin gene was PCR amplified with primer 5 and primer 6. Plasmid vector pBAD/His C and PCR amplified products were digested with *Pst*I and *Hind*III. These digested products were further ligated to produce a recombinant construct pJSM3. Further, all the above recombinant plasmids were transformed in *E. coli* DH5$\alpha$ cells with standard protocol.

## Protein expression and purification

Expression and purification of *hipBA*$^{Xn2}$ TA proteins were analyzed in *E. coli* cells. For this, recombinant constructs pJSM1 and pJSM3 were transformed into *E. coli* TOP10 cells and pJSM2 was transformed into *E. coli* BL21 (DE3) cells. The primary culture was prepared by inoculating transformed cells in LB broth supplemented with 100µg/mL Ampicillin (JSM1 and JSM3) or 50µg/mL Kanamycin (JSM2) and incubated at 37°C for overnight. 1% v/v of primary culture was used in 50ml LB broth for preparing secondary culture incubated at 37°C with a 220 rpm shaking condition. In the case of JSM1 and JSM3, culture was induced with 0.2% of L-arabinose while for JSM2; it was induced with 1mM of isopropyl-β-D-thiogalactopyranoside (IPTG), at the $OD_{600}$ value of 0.5 for 6 hours. 50mL of induced culture was harvested and pelleted to dissolve in 10 mL of lysis buffer (50 mM $NaH_2PO_4$, 300 mM NaCl, pH 8.0). To prepare a total cell lysate, cells were sonicated on ice for 20 cycles (10 s on/off) and centrifuged at 12,000 x g for 30 minutes at 4˚C. Ni-NTA affinity chromatography was used to separate recombinant HipA$^{Xn}$ toxin and HipB$^{Xn}$ antitoxin proteins. Supernatant having soluble proteins was loaded on the Ni-NTA superflow column (Qiagen). After passing proteins, column was washed with washing buffer (50 mM $NaH_2PO_4$, 300mM NaCl, 20 mM Imidazole, pH 8.0) and *hipBA*$^{Xn2}$proteins were eluted by 15 mL of elution buffer (50 mM $NaH_2PO_4$, 300 mM NaCl, 250 mM Imidazole, pH 8.0). These eluted proteins were dialyzed against dialysis buffer (50 mM $NaH_2PO_4$, 300 mM NaCl, 2 mM β-mercaptoethanol, 20% glycerol, pH 8.0) at 4˚C overnight. Thermo Scientific™ NanoDrop 2000 was utilized for measuring the purity and concentration of these purified proteins. Further, these purified proteins were analyzed on 15% sodium dodecyl sulfate-polyacrylamide gel electrophoresis (SDS-PAGE) and confirmed by Western blotting probed with mouse anti-His monoclonal primary antibody (Bio-Rad, USA) as per the protocol described elsewhere (Mohit Yadav & Jitendra Singh Rathore 2020).

## Toxicity assessment

The toxicity assessment was performed in liquid and solid LB medium. Recombinant constructs pJSM1 and pJSM3 have transformed into *E. coli* TOP 10 cells resulting in JSM4 and JSM5 strains. These strains were inoculated in liquid LB medium supplemented with 100µg/mL of ampicillin and incubated at 37°C overnight with a 220 rpm shaking condition. For assay toxicity in the liquid medium, overnight grown culture of JSM4 and JSM5 was inoculated with 1:100 in LB medium and incubated at 37°C. Cultures were induced with 0.2% of L-arabinose at the $OD_{600}$ of 0.1. Samples were harvested at each hour post-induction and $OD_{600}$ was measured with a spectrophotometer (Perkin Elmer, Waltham, MA). For assay toxicity on solid medium, these harvested samples were serially diluted and spotted on LB agar plates containing 100µg/mL of ampicillin. After overnight incubation at 37°C, colony-forming units (CFU) were counted. Mean value of three independent experiments were used to show the growth parameters at different interval of time.

## Site-directed mutagenesis

Site-directed mutagenesis at the active site residues of *hipA*$^{Xn2}$ toxin was performed by following the protocol as described elsewhere (Singh 2013; Yadav and Rathore 2020). Primers used are listed in Table S2. Active site residues Gly-8, Ser-129, His-164, Asn-167, Ser-169, Asp-185, and Thr-220 were substituted with alanine. In brief, the pJSM1 construct was used as a template and mutated in pG8A, pS129A, pH164A, pN167A, pS169A, pD185A, and pT220A recombinant plasmid constructs. These recombinant constructs were transformed in *E. coli* TOP10 cells using a standard protocol and resulted in mutants G8A, S129A, H164A, N167A, S169A, D185A, and T220A as described in table 1. Further, we also performed the toxicity assessment of mutants and wild type *hipA*$^{Xn2}$ toxin by following the method as described before in materials and methods.

## Reporter assay

For the reporter *β-galactosidase* assay, 529 bp upstream region of the *hipBA*$^{Xn2}$ TA system was used as the promoter. The method for determining *β-galactosidase* assay was used as described elsewhere (Yadav and Rathore 2018a, 2020). In brief, constructs/strains used in this study are listed in Table S1 and primer sequences details are given in Table S2. Promoter activity in different stress conditions (elevated temperature, antibiotic, and nutrient starvation) was measured and expressed in Miller units (MU) (Miller 1972). The *hipBA*$^{Xn2}$ TA promoter was cloned in the pGEM-T Easy vector and resulting in the JSM6 strain containing the promoter-*lacZ* fusion. For primary culture, the fusion construct was incubated overnight at 30°C with 220 rpm shaking in LB medium supplemented with 100µg/mL ampicillin. 1:100 of primary culture was inoculated in secondary culture with LB media and incubated at 30°C. All samples were exposed to different stress conditions at $OD_{600}$ of 0.1 and promoter activity was measured.

## Reverse Transcriptase Polymerase Chain Reaction (RT-PCR)

Total RNA and RT-PCR analysis from *X. nematophila* were performed by following the method as described previously (Yadav and Rathore 2018b; Mohit Yadav & Jitendra Singh Rathore 2020). In brief, 1% of the overnight *X. nematophila* culture was inoculated in nutrient broth and subjected to different stress conditions described as elevated temperature, antibiotic, and nutrient starvation. At different time intervals, cells were harvested and total RNA was isolated for RT-PCR analysis. Primer details for RT-PCR are given in Table S2. A sequence of 16s RNA from *X. nematophila* was used as a control gene. One-step RT-PCR kit (Qiagen) was utilized for this analysis. PCR reaction included 80 ng RNA (DNase treated), 10 mM of deoxynucleoside triphosphate (dNTP) mixture, 5 mM of primers, 5.0 µL of RT-PCR buffer and l µL of enzyme mixture in 50 µL reactions. PCR was analyzed on 1 % agarose gel by EtBr staining.

### Gel Shift Assay

Gel shift assay was performed as described elsewhere (Mohit Yadav & Jitendra Singh Rathore 2020). Purified recombinant HipA$^{Xn2}$ toxin and HipB$^{Xn2}$ antitoxin proteins dialyzed against 1X assay buffer (1.8M NaCl pH 7.5, 1M Tris pH 7.2, 1% SDS) and concentrated by Amicon Ultra-0.5 device (Merck). The promoter region of the *hipBA*$^{Xn2}$ TA system (529 bp) was amplified and purified as described before in materials and methods. A concentration gradient of purified HipA$^{Xn2}$ toxin and HipB$^{Xn2}$ antitoxin proteins was incubated with 250 ng of purified promoter DNA containing 1X assay buffer for 30 minutes at room temperature. These prepared samples were analyzed on 8% Native PAGE gel at 4˚C. Gels were visualized by Ethidium bromide (EtBr) dye.

# Results

### Genetic organization of a putative *hipBA*$^{Xn2}$ TA system

A homolog of *hipBA* TA system in the genome of *X. nematophila* ATCC 19061 (NCBI Refseq NC_014228) was identified at position 3774379-3775635 bp on the negative strand under XNC1_operon 0746 locus tag and named as *hipBA*$^{Xn2}$ TA system. This TA system was comprised of an 813 bp *hipA*$^{Xn2}$ toxin gene which encodes for a 270 amino-acid residue protein and a 408 bp *hipB*$^{Xn2}$ antitoxin gene which encodes for a protein having 135 amino acids as shown in Fig. 1. The chromosomal location of the *hipA*$^{Xn2}$ toxic gene was 3774379-3775191 bp with locus tag XNC1_3911 and the *hipB*$^{Xn2}$ antitoxin gene was positioned at 3775228-3775635 bp with locus tag XNC1_3912. The intragenic space between these two genes was 37 bp. Upstream region of the *hipB*$^{Xn2}$ antitoxin gene was also explored for the predicted 529 bp promoter entity of the *hipBA*$^{Xn2}$ TA system with -10 box 5’TGCTATTAT3’ having a score of 74 and -35 box 5’TTACAA3’ having a score of 32 as depicted in Fig. 1. Binding sites for transcription factors *ihf* and *rpo*S17 were also identified in this promoter region with sequences 5’AATAAAAT3’ and 5’CTATTATA3’ respectively as illustrated in Fig. 1.

### Phylogenetic analysis of HipA$^{Xn2}$ toxin and HipB$^{Xn2}$ antitoxin

To relate the homolog of the *hipBA* TA system, a detailed phylogenetic analysis was performed at the protein level for the *hipBA*$^{Xn2}$ TA system. Based on BLASTP algorithm results, for HipA$^{Xn2}$ toxin phylogenetic analysis, different bacteria namely, *Photorhabdus luminescens*, *Xenorhabdus khoisanae*, *Lelliottia amnigena*, *Morganella morganii*, *Morganella psychrotolerans*, *Cedecea neteri*, *Klebsiella pneumoniae*, *Serratia marcescensEnterobacter sp*. 638 and *E. coli* were selected as the source of different serine/threonine protein kinases. These kinases had a higher degree of similarity with HipA$^{Xn2}$ toxin as illustrated in Fig. 2a. Closely related bacterium *Photorhabdus luminescens'* kinase forms a separate cluster with HipA$^{Xn2}$ toxin and it was found that HipA$^{Xn2}$ toxin was more closely related to kinase from *E. coli* with a clade credibility value of 100. However, distantly related kinases from *Morganella psychrotolerans* and *Xenorhabdus khoisanae* had their separate cluster with a clade credibility value of 92 as depicted in Fig. 2a. Similarly, for HipB$^{Xn2}$ antitoxin phylogenetic analysis, according to BLASTP results, a series of transcriptional regulatory proteins from different bacteria namely *Xenorhabdus szentirmaii*, *Photorhabdus luminescens*, *Xenorhabdus khoisanae*, *Xenorhabdus eapokensis*, *Halomonas saccharevitans*, *Edwardsiella hoshinae,Leclercia adecarboxylata*, *Salinicola sp*. MIT1003 and *E. coli* were screened. These regulatory proteins had a higher degree of similarity to HipB$^{Xn2}$ antitoxin as shown in Fig. 2b. The proximity of HipB$^{Xn2}$ antitoxin was found with the transcriptional regulatory protein of *E. coli* having a clade credibility value of 98 while it was more distantly related to the regulatory protein of *Leclercia adecarboxylata* with a clade credibility value of 87 as depicted in Fig. 2b.

## Structural assessment of HipA$^{Xn2}$ toxin and HipB$^{Xn2}$ antitoxin

To characterize the *hipBA*$^{Xn2}$ TA system, both identified TA proteins were structurally modeled as depicted in Fig.2. Multiple templates for these models were analyzed by LOMETS from the PDB library. Z-score was calculated to measure the significance of the models. For HipA$^{Xn2}$ toxin, 4pu3A was the most significant template with a normalized Z-score of 1.18 as illustrated in Fig. 2a and for HipB$^{Xn2}$ antitoxin, it was 1b0nA with a normalized Z-score 1.52 as shown in Fig. 2b. Further, these models were characterized based on C-score, TM-score, and RMSD. For the HipA$^{Xn2}$ toxin model, C-score was 0.85 and other parameters including TM-score and RMSD were 0.61±0.14 and 7.9±4.4Å respectively. While for HipB$^{Xn2}$ antitoxin model C-score was 3.17 and other parameters including TM-score and RMSD were 0.36±0.12 and 11.8±4.5Å respectively. Moreover, Protein Structure Validation Software Suit (PSVS version 1.5) was also used to validate these models. Ramachandran plot analysis and statistics showed that 75.70 % of residues in the HipA$^{Xn2}$ model were in the favored regions and 93.80 % in the allowed regions as described in Fig 2a. In the case of the HipB$^{Xn2}$ model, 75.20 % residues were in the favored region and 94.70 % in the allowed regions as shown in Fig 2b.

## Expression and purification analysis of *hipBA*$^{Xn2}$TA system proteins

Different recombinant constructs were developed for the expression and purification study of HipA$^{Xn2}$ toxin and HipB$^{Xn2}$ antitoxin from *X. nematophila,* and details are described in Table S1. *E. coli* cells were used as host cells for this purpose due to its lavishly controlled expression features (Ning et al. 2013;

Zheng et al. 2017; Thomet et al. 2019). *hipA*$^{Xn2}$ toxin gene with a size of 813 bp that encoding a 31.04 kDa protein was cloned in pBAD/His C vector for its tight regulation attribute. The expression profile of the *hipA*$^{Xn2}$ toxin gene (recombinant strain JSM4) was analyzed on 15% SDS-PAGE as depicted in Fig. 3a. As the protein band of HipA$^{Xn2}$ toxin was not clearly distinguished in the total lysate (lane TL) therefore, under native conditions, HipA$^{Xn2}$ toxin protein was purified with Ni-NTA affinity chromatography and a clear single band was detected in the fractions E1 to E6 at ~31 kDa that ratified the size of the recombinant HipA$^{Xn2}$ toxin protein with 6XHis-tag as shown in Fig. 3a.

Further, the alone *hipB*$^{Xn2}$ antitoxin gene (408 bp) encoding the 14.90 kDa protein was cloned under the strong T7 promoter in the pET28a vector with N-terminal 6XHis-tag. To study the expression level of the *hipB*$^{Xn2}$ antitoxin gene, recombinant strain JSM7 was used and the expression profile was observed as illustrated in Fig. 3b. A band labeled with *hipB*$^{Xn2}$ antitoxin was not distinct in the total lysate (lane TL), therefore after purification with Ni-NTA affinity chromatography under native conditions, a single band was observed in the fractions E1 to E6 at ~15 kDa that corroborate with the size of the recombinant HipB$^{Xn2}$ antitoxin having 6XHis-tag as shown in Fig. 3b.

The same approach was also used to clone the *hipBA*$^{Xn2}$ operon comprised of *hipA*$^{Xn2}$ toxin and *hipB*$^{Xn2}$ antitoxin genes in *cis*-form and expression profile with recombinant strain JSM5 of both genes was illustrated in Fig. 3c. As the protein bands of HipA$^{Xn2}$ toxin and HipB$^{Xn2}$ antitoxin were not differentiable in the total lysate (lane TL) and thus, after purification, under native conditions by using Ni-NTA affinity chromatography, distinguishable bands of HipA$^{Xn2}$ toxin and HipB$^{Xn2}$ antitoxin proteins were observed in the fractions from E1 to E6 at ~31 kDa and ~15 kDa which varified the size of the recombinant HipA$^{Xn2}$ toxin and HipB$^{Xn2}$ antitoxin proteins with 6XHis-tag as shown in Fig. 3c. These purified recombinant HipA$^{Xn2}$ toxin and HipB$^{Xn2}$ antitoxin proteins were further detected by Western blot analysis. A single-band was observed at a size of ~31 kDa and ~15 kDa which ratified the size of the recombinant HipA$^{Xn2}$ toxin protein and HipB$^{Xn2}$ antitoxin proteins respectively, as shown in Fig. 3d.

## Functional assessment of *hipBA*$^{Xn2}$ TA system

Recombinant strains JSM4 and JSM5 containing *hipA*$^{Xn2}$ toxin and *hipA*$^{Xn2}$-*hipB*$^{Xn2}$ TA complex genes respectively were used to analyze the functionality of *hipBA*$^{Xn2}$ TA system. We observed the growth profiles of these strains after the overexpression of *hipA*$^{Xn2}$ toxin and *hipA*$^{Xn2}$-*hipB*$^{Xn2}$ TA genes in liquid and on solid medium. In liquid media, post-induction, at each hour $OD_{600}$ was measured and *E. coli* Top10 cells with an empty pBAD/His C vector was used as a control as depicted in Fig. 4a. After 3h of induction, it was observed that cells overexpressing HipA$^{Xn2}$ toxin inhibit the growth by two-fold as compared to control cells and as induction time increased, a sudden increment in the growth of control cells was also noticed and thus, after 4h to 7h of induction, the growth of cells containing *hipA*$^{Xn2}$ toxin gene was retarded by more than 2.5-fold as compared to control as illustrated in Fig 4a.

While a different growth profile pattern was observed in cells overexpressing *hipBA*$^{Xn2}$ TA complex genes as shown in Fig. 4a, due to the effect of HipB$^{Xn2}$ antitoxin on HipA$^{Xn2}$ toxin. At an initial 2h of post-induction, the toxicity of HipA$^{Xn2}$ toxin was not significantly neutralized by HipB$^{Xn2}$antitoxin, but a clear effect of HipB$^{Xn2}$ antitoxin overexpression was observed from 3rd hour of induction as depicted in Fig. 4a. After 3h to 7h of post-induction, it was found that the cellular growth of *hipBA*$^{Xn2}$ TA complex genes harboring cells was resumed by more than two-fold as compared to only the *hipBA*$^{Xn2}$ toxin gene-containing cells. Additionally, these observations were supported by growth assay on solid media as depicted in Fig. 4b. Colony-forming units (CFU) of recombinant strains JSM4, JSM5, and control cells were calculated. At the beginning of 3h post-induction, CFU counts of these strains were almost similar although in later hour *i.e.* after 4h to 7h, due to overexpression of HipA$^{Xn2}$ toxin in JSM4, the number of viable cells was declined as compared to JSM5 and control cells as depicted in Fig. 4b. All experiments were conducted three times to verify the observations.

## Determination of active site residues responsible for the toxicity of HipA$^{Xn2}$ toxin

To access the function of active site residues in HipA$^{Xn2}$ toxin, we have performed site-directed mutagenesis (SDM) and followed a toxicity assay analysis. Active site residues were screened by bioinformatics analysis as described elsewhere (Mohit Yadav & Jitendra Singh Rathore 2020) and by sequence alignment with other bacterial pathogens as depicted in Fig. 5. The selected active site residues were Gly-8, Ser-129, His-164, Asn-167, Ser-169, Asp-185, and Thr-220, as shown in Fig. 6a and these were substituted with alanine to avoid any structural complexity. In toxicity assay analysis, we have included mutant strains G8A, S129A, H164A, N167A, S169A, D185A, T220A, a control (*E. coli* cells with empty pBAD/His C vector) and a wild type (WT) strain *i.e.E. coli* cells harboring pBAD/His C *hipA*$^{Xn}$ toxin (for details see Table S1). Initial 3h of post-induction, all mutants and WT were shown almost a similar growth profile pattern however from the fourth hour onwards mutants G8A, H164A, N167A, and S169A were showing elevated growth level compare to WT strain and approaches to the control as shown in Fig. 6b. Mutants S129A, D185A, and T220A were not significantly different from the growth pattern of WT strain throughout the growth study. In 4$^{th}$ hour, percent growth inhibition for strain G8A, H164A, N167A, S169A, and WT was 46.34%, 41.46%, 56.09%, 46.34%, and 61.5% respectively as compared to control and in 5$^{th}$ hour, percent growth inhibition for these strains was reached to 53.81%, 50.26%, 57.37%, 53.81%, and 65% respectively as compared to control. While in 6$^{th}$ hour, percent growth inhibition for strain G8A, H164A, N167A, S169A, and WT were estimated to 50%, 43.70%, 47%, 47%, and 63% respectively as compared to control and in 7$^{th}$ hour, this was approaching to 41.17%, 31.88%, 38.08%, 31.88%, and 50%.

Further, we examined these results by evaluating viable cells on solid LB media as illustrated in Fig. 6c. We determined the colony-forming units (CFU) of *E. coli* cells overexpressing HipA$^{Xn2}$ toxin and its mutants. After induction, at each hour, samples were harvested and diluted to spot on the LB medium. With overnight incubation at 37ºC, CFUs were counted and plotted against time post-induction. There was no significant difference observed in CFU counts of mutants S129A, D185A, and T220A as compared to WT as shown in Fig. 6c. While, from an initial 2h of post-induction, mutants G8A, H164A, N167A, and

S169A were exhibiting increased CFU counts as compared to WT as depicted in Fig. 6c. In the 6-7h of post-induction, the CFU counts for these mutants were approaching the control and it was increased with more than 1.5-fold as compared to WT. Thus, the absorbance and viable cell count results show that four active site residues namely, Gly-8, His-164, Asn-167, and Ser-169 are crucial for the toxicity of *hipA*$^{Xn2}$ toxin.

## Transcriptional regulation of *hipBA*$^{Xn2}$ TA system under stress conditions

To analyze the transcription regulation of the *hipBA*$^{Xn2}$ TA module under stress conditions like elevated temperature, antibiotics, and nutrient starvation, we have cloned 529 bp promoter sequences in reporter plasmid pJSM6. Thus, the β-galactosidase activity of the *hipBA*$^{Xn2}$ TA promoter, in *E. coli* strain JSM6, was measured in the form of Miller unites (MUs) (Miller 1972) as illustrated in Fig. 7. This MUs examination was further confirmed by Reverse Transcriptase Polymerase Chain Reaction (RT-PCR) analysis in *X. nematophila* as depicted in Fig. 7. In this analysis, loading control was 16s RNA gene from *X. nematophila,* while primer details and gene sizes are depicted in Fig. 7a.

Under elevated temperature conditions, after two hours of incubation at 42˚C, the promoter activity was increased by three-fold and at 37˚C it was higher as compared to 30˚C as shown in Fig. 7b. In the RT-PCR analysis, this up-regulation was validated by observed higher intensity bands of *hipA*$^{Xn2}$ toxin*, hipB*$^{Xn2}$ antitoxin, and *hipBA*$^{Xn2}$ operon genes under these temperature conditions as shown in Fig. 7e. For antibiotics stress conditions, two antibiotics ciprofloxacin and ofloxacin were used. The concentration of antibiotics dose were 1 and 3 µg/mL as described in our previous studies (Yadav and Rathore 2018; Mohit Yadav & Jitendra Singh Rathore 2020). Higher promoter activity was observed after the 20 minutes of ofloxacin administration while it was activated by almost two-fold in the case of ciprofloxacin treatment as compared to control cells (without antibiotics) depicted in Fig. 7c. Under the same conditions, RT-PCR analysis of *hipA*$^{Xn2}$ toxin*, hipB*$^{Xn2}$ antitoxin, and *hipBA*$^{Xn2}$ operon genes was also performed, and up-regulation was further confirmed by intense bands as shown in Fig. 7f.

Nutrient starvation conditions were generated as described elsewhere (Yadav and Rathore 2018a; Mohit Yadav & Jitendra Singh Rathore 2020). Under these conditions, it was estimated that promoter activity was decreased by two-fold as compared to activity in M9 medium of stressed condition as illustrated in Fig. 7d. This down-regulation was further validated with low-intensity RT-PCR bands of *hipA*$^{Xn2}$ toxin*,* *hipB*$^{Xn2}$ antitoxin, and *hipBA*$^{Xn2}$ operon genes as shown in Fig. 7g.

## Interaction analysis of recombinant *hipBA*$^{Xn2}$ TA proteins with its promoter

The regulation of the *hipBA*$^{Xn2}$ TA system was further investigated by analyzing the interaction of recombinant HipA$^{Xn2}$ toxin and HipB$^{Xn2}$ antitoxin proteins with its promoter region. A gel shift assay was performed with 200 ng of purified 529 bp *hipBA*$^{Xn2}$ promoter and a concentration gradient (0.25 to 1.5 µM) of purified recombinant HipA$^{Xn2}$ toxin and HipB$^{Xn2}$ antitoxin proteins as illustrated in Fig. 8. There was no interaction observed, when the *hipBA*$^{Xn2}$ TA promoter was subjected to recombinant HipA$^{Xn2}$ toxin

protein as depicted in Fig. 8a. However, in the case of recombinant HipB$^{Xn2}$ antitoxin protein, a clear shift of the *hipBA$^{Xn2}$* TA promoter band was observed in the range of 0.25 to 1.0 µM of antitoxin protein as shown in Fig. 8b; and when we added both recombinant HipA$^{Xn2}$ toxin and HipB$^{Xn2}$ antitoxin proteins of 0.25 to 1.5 µM concentration range to the promoter, the band intensity of shift was further increased as shown in Fig. 8c. For control, we used non-interacting Bovine Serum Albumin (BSA) protein in the same concentration range to interact with the *hipBA$^{Xn2}$* TA promoter and no shift was found as illustrated in Fig. 8d.

# Discussion

Under stressful environmental conditions in particular oxidative stress, nutritional depletion, temperature variation, etc., TA systems have differentially induction phenomena (Huang et al.; Ramage et al. 2009; Singh et al. 2010). The genome of *X. nematophila* has a copious amount of TA systems (Yadav and Rathore 2018) that make the basis to explore their role in its physiology. The *X. nematophila* ATCC 19061 chromosome contains three *hipBA* TA homolog operons (Yadav and Rathore 2018) (*hipBA$^{Xn}$*, *hipBA$^{Xn2}$*, and *hipBA$^{Xn3}$*) and possibly each will have a different effect on bacterial growth, molecular structure, expression profile, gene regulation pattern and cellular viability. Among these three operons, previously, *hipBA$^{Xn}$* TA operon was identified as a *bonafide* type II TA system and the *hipBA$^{Xn3}$* TA system was a *pseudo*-type TA system (Yadav and Rathore 2018; Mohit Yadav & Jitendra Singh Rathore 2020) and the role of *hipBA$^{Xn2}$* TA system was unknown.

Thus, the present study was conducted to investigate the activity of the second *hipBA* TA homolog operon named as *hipBA$^{Xn2}$* TA system from *X. nematophila*. Here, we identified the chromosomal location of the *hipBA$^{Xn2}$* TA system (Fig. 1) and by phylogenetic analysis, we confirmed that the *hipA$^{Xn2}$* gene encoded a serine/threonine-protein kinase (HipA$^{Xn2}$ toxin) while *hipB$^{Xn2}$* gene encoded a transcriptional regulatory protein (HipB$^{Xn2}$ antitoxin) as depicted in Fig. 2. Further, we analyzed the heterologous overexpression and purification of recombinant HipA$^{Xn}$ toxin and HipB$^{Xn}$ antitoxin proteins in a lavishly controlled *E. coli* expression system (Deep et al. 2018; Thomet et al. 2019; Yadav and Rathore 2020) (Fig. 3). As expected, heterologous overexpression of HipA$^{Xn2}$ toxin in *E. coli* cells majorly retard the growth of these cells, and the toxicity of this toxin was neutralized when it was co-expressed with its cognate HipB$^{Xn2}$ antitoxin partner (Fig. 4), these results are consistent with our previous findings of first validated *hipBA$^{Xn}$* TA system (Yadav and Rathore 2020). To further elucidate the function of HipA$^{Xn2}$ toxin, we constructed various mutant strains devoid of activity associated with this toxin. In HipA toxin from *E. coli*, residues Gly-22, Asp-88, Ser150, Asp-291, Asp-309, and Asp-332 were very crucial for its activity (Leberman et al. 1980; Korch et al. 2003; Correia et al. 2006; Kaspy et al. 2013; Schumacher et al. 2015) while residues Ser149, Asp-306, and Asp-329 had great importance in the activity of HipA$^{Xn}$ toxin (Yadav and Rathore 2020). Thus, it was much needed to explore the role of such residues in HipA$^{Xn2}$ toxin and we found that four residues Gly-8, His-164, Asn-167, and Ser-169 are very essential for its toxicity as shown in Fig. 6.

TA systems are known as stress-adaptive entities and our observation that the *hipBA*$^{Xn2}$ TA system is activated under different adverse conditions (Fig. 7) supports the perception that this TA locus contributes to *X. nematophila* physiology. For instance, the increases in *hipBA*$^{Xn2}$ TA transcripts in *X. nematophila* upon exposure to elevated temperature, nutrient starvation, and antibiotics (Fig.7) indicate that this TA might play a pivotal role in bacterial adaptation to such conditions. The regulated activation of TA systems in similar stress associated conditions has also been observed (Gupta et al. 2017; Yadav and Rathore 2020). RT–PCR analysis exhibited the distinctive induction profile of the *hipBA*$^{Xn2}$ TA system, and under most of the stress environment tested, the levels of *hipA*$^{Xn2}$ toxin transcripts were higher than the levels of their cognate *hipB*$^{Xn2}$ antitoxin transcripts as illustrated in Fig. 7. Such divergence in the transcript extents may be due to the distinctive stability of the transcripts or the expression of *hipA*$^{Xn2}$ toxin is driven from multiple promoters. Likewise, post-transcriptional regulation of TA modules has also been reported (Singh et al. 2010; Yadav and Rathore 2020).

Transcriptional control of the *hipBA*$^{Xn2}$ TA system was further supported by the gel shift assay as shown in Fig. 8. The mobility of the *hipBA*$^{Xn2}$ TA promoter was hindered by HipB$^{Xn2}$ antitoxin and HipBA$^{Xn2}$ toxin-antitoxin while alone HipA$^{Xn2}$ toxin does not affect its mobility as illustrated in Fig. Therefore, HipB$^{Xn}$ antitoxin may be a repressor protein in the transcriptional regulation of the *hipBA*$^{Xn2}$ TA system whereas the association of HipA$^{Xn2}$ toxin protein in it works as a corepressor. Similarly, Transcriptional control studies have also been done before in different TA systems that also support our assumptions (Overgaard et al. 2008; Kędzierska and Hayes 2016; Yadav and Rathore 2020). According to these observations, a proposed transcription regulation model of all three *hipBA* TA homologs from *X. nematophila* is illustrated in Fig. 9.

As *hipBA*$^{Xn3}$ is a *pseudo*-type TA system, thus, the distinct response of *hipBA*$^{Xn}$ and *hipBA*$^{Xn2}$ TA systems most likely suggests the components of TA systems have different substrates or specificity for their activity. Other TA systems like *parDE, mazEF,* and *hipBA* in *E. coli* have been studied for different substrates or specificity (Huang et al.; Zhang et al. 2003; Monti et al. 2007). Therefore, by these results, it may be conceptualized that each TA system has separate and defined interactome to produce a differential effect of TAs in bacterial physiology. Moreover, the multiple numbers of TA loci in *X. nematophila* may hence reflect the necessity for extra control over the general expression of typical protein subsets as compare to having less or no TAs such as *E. coli*, which has only 5 TA systems (Pandey and Gerdes).

Future experiments include identifying cellular targets for *hipBA*$^{Xn2}$ TA and elucidating the roles of these TA systems in *X. nematophila* persistence. Conclusively, we have been revealed some crucial points regarding *hipBA*$^{Xn}$ TA system such as it is an organized operon with two genes, both genes are protein in nature in which one encodes a toxin and other encodes an antitoxin, toxin protein inhibits the bacterial growth while antitoxin protein neutralized it, the formation of a TA complex, and activation of this TA system in stress conditions. All these attributes a typical type II TA system (Yamaguchi et al. 2011; Ghafourian et al. 2014) and thus *hipBA*$^{Xn2}$ TA system is an active type II TA system.

# Declarations


### Acknowledgments

Mohit Yadav received a senior research fellowship (SRF) from the Council of Scientific & Industrial Research (CSIR), India. This research work was financially supported by the Council of Scientific & Industrial Research (CSIR), India, through project no. 37(1658)/15-EMR-II to Dr. Jitendra Singh Rathore.

**Funding** This study was funded by the Council of Scientific & Industrial Research (CSIR), India, through project no. 37(1658)/15-EMR-II to Dr. Jitendra Singh Rathore.


**Conflicts of interest** The authors declare that they have no conflict of interest.

**Ethics approval** This is an observational study. The GBU Research Ethics Committee has confirmed that no ethical approval is required.

**Consent to participate** Not applicable

**Consent for publication** Not applicable

**Availability of data and material** All data generated or analyzed during this study are included in this published article [and its supplementary information files].

**Code availability** Not applicable

**Authors' contributions** Conceptualization: Mohit Yadav and Jitendra Singh Rathore; Methodology: Mohit Yadav Formal analysis and investigation: Jitendra Singh Rathore Writing - original draft preparation: Mohit Yadav; Writing - review and editing: Jitendra Singh Rathore; Funding acquisition: Mohit Yadav and Jitendra Singh Rathore; Resources: Jitendra Singh Rathore; Supervision: Jitendra Singh Rathore

# References


1. Akarsu H, Bordes P, Mansour M, et al (2019) TASmania: A bacterial Toxin-Antitoxin Systems database. PLOS Comput Biol 15:e1006946. https://doi.org/10.1371/journal.pcbi.1006946
2. Bentley SD, Chater KF, Cerdeño-Tárraga A-M, et al (2002) Complete genome sequence of the model actinomycete *Streptomyces coelicolor* A3(2). Nature 417:141–147. https://doi.org/10.1038/417141a
3. Boutte CC, Crosson S (2013) Bacterial lifestyle shapes stringent response activation. Trends Microbiol. 21:174–180
4. Chaston JM, Suen G, Tucker SL, et al (2011) The entomopathogenic bacterial endosymbionts *Xenorhabdus* and *Photorhabdus*: convergent lifestyles from divergent genomes. PLoS One 6:e27909. https://doi.org/10.1371/journal.pone.0027909
5. Correia FF, D'Onofrio A, Rejtar T, et al (2006) Kinase activity of overexpressed HipA is required for growth arrest and multidrug tolerance in *Escherichia coli*. J Bacteriol 188:8360–7.

https://doi.org/10.1128/JB.01237-06

6. Deep A, Tiwari P, Agarwal S, et al (2018) Structural , functional and biological insights into the role of *Mycobacterium tuberculosis* VapBC11 toxin – antitoxin system : targeting a tRNase to tackle mycobacterial adaptation. 1–17. https://doi.org/10.1093/nar/gky924
7. Gerdes K, Maisonneuve E (2012) Bacterial persistence and toxin-antitoxin loci. Annu Rev Microbiol 66:103–123. https://doi.org/10.1146/annurev-micro-092611-150159
8. Ghafourian S, Raftari M, Sadeghifard N, Sekawi Z (2014) Toxin-antitoxin Systems: classification, biological function and application in biotechnology. Curr Issues Mol Biol 16:9–14
9. Gopalakrishnan K, Sowmiya G, Sheik SS, Sekar K (2007) Ramachandran plot on the web (2.0). Protein Pept Lett 14:669–71
10. Gupta A, Venkataraman B, Vasudevan M, Gopinath Bankar K (2017) Co-expression network analysis of toxin-antitoxin loci in *Mycobacterium tuberculosis* reveals key modulators of cellular stress. Sci Rep 7:5868. https://doi.org/10.1038/s41598-017-06003-7
11. Huang charlie Y, Gonzalez-Lopez carlos, Henry céline, et al *hipBA* toxin-antitoxin systems mediate persistence in *Caulobacter crescentus.* https://doi.org/10.1038/s41598-020-59283-x
12. Kaspy I, Rotem E, Weiss N, et al (2013) HipA-mediated antibiotic persistense via phosphorylation of the glutamyl-tRNA-synthetase. Nat Commun 4:3001. https://doi.org/10.1038/ncomms4001
13. Katoh K, Standley DM (2013) MAFFT multiple sequence alignment software Vvrsion 7: improvements in performance and usability. Mol Biol Evol 30:772–780. https://doi.org/10.1093/molbev/mst010
14. Kędzierska B, Hayes F (2016) Emerging roles of toxin-antitoxin modules in bacterial pathogenesis. Molecules 21:790. https://doi.org/10.3390/molecules21060790
15. Korch SB, Henderson TA, Hill TM (2003) Characterization of the *hipA*7 allele of *Escherichia coli* and evidence that high persistence is governed by (p)ppGpp synthesis. Mol Microbiol 50:1199–1213. https://doi.org/10.1046/j.1365-2958.2003.03779.x
16. Kumar S, Stecher G, Li M, et al MEGA X: Molecular evolutionary genetics analysis across computing platforms. https://doi.org/10.1093/molbev/msy096
17. Leberman R, Antonsson B, Giovanelli R, et al (1980) A simplified procedure for the isolation of bacterial polypeptide elongation factor EF-Tu. Anal Biochem 104:29–36. https://doi.org/10.1016/0003-2697(80)90272-9
18. Mahmood S, Kumar M, Kumari P, et al (2020) Novel insecticidal chitinase from the insect pathogen *Xenorhabdus nematophila*. Int J Biol Macromol. https://doi.org/10.1016/j.ijbiomac.2020.05.078
19. Maisonneuve E, Castro-Camargo M, Gerdes K (2013) (p)ppGpp controls bacterial persistence by stochastic induction of toxin-antitoxin activity. Cell 154:. https://doi.org/10.1016/j.cell.2013.07.048
20. Manganelli R, Proveddi R, Rodrigue S, et al (2004) σ factors and global gene regulation in *Mycobacterium tuberculosis*. J. Bacteriol. 186:895–902

21. Martens EC, Heungens K, Goodrich-Blair H (2003) Early colonization events in the mutualistic association between *Steinernema carpocapsae* nematodes and *Xenorhabdus nematophila* bacteria. J Bacteriol 185:3147–54. https://doi.org/10.1128/JB.185.10.3147-3154.2003
22. Miller JH (1972) Experiments in molecular genetics. Cold Spring Harbor Laboratory
23. Mohit Yadav & Jitendra Singh Rathore (2020) The *hipBA*$^{Xn}$ operon from *Xenorhabdus nematophila* functions as a bonafide toxin-antitoxin module. Appl Microbiol Biotechnol. https://doi.org/10.1007/s00253-020-10441-1
24. Monti MC, Hernández-Arriaga AM, Kamphuis MB, et al (2007) Interactions of Kid-Kis toxin-antitoxin complexes with the parD operator-promoter region of plasmid R1 are piloted by the Kis antitoxin and tuned by the stoichiometry of Kid-Kis oligomers. Nucleic Acids Res 35:1737–49. https://doi.org/10.1093/nar/gkm073
25. Ning D, Jiang Y, Liu Z, Xu Q (2013) Characterization of a Chromosomal Type II Toxin–Antitoxin System mazEaFa in the *Cyanobacterium anabaena* sp. PCC 7120. PLoS One 8:e56035. https://doi.org/10.1371/journal.pone.0056035
26. Overgaard M, Borch J, Jørgensen MG, Gerdes K (2008) Messenger RNA interferase RelE controls *relBE* transcription by conditional cooperativity. Mol Microbiol 69:841–857. https://doi.org/10.1111/j.1365-2958.2008.06313.x
27. Page R, Peti W (2016) Toxin-antitoxin systems in bacterial growth arrest and persistence. Nat Chem Biol 12:208–214. https://doi.org/10.1038/nchembio.2044
28. Pandey DP, Gerdes K Toxin-antitoxin loci are highly abundant in free-living but lost from host-associated prokaryotes. https://doi.org/10.1093/nar/gki201
29. Park Y, Kim Y (2000) Eicosanoids rescue Spodoptera exigua infected with *Xenorhabdus nematophilus,* the symbiotic bacteria to the entomopathogenic nematode *Steinernema carpocapsae.* J Insect Physiol 46:1469–1476. https://doi.org/10.1016/S0022-1910(00)00071-8
30. Ramage HR, Connolly LE, Cox JS (2009) Comprehensive functional analysis of *Mycobacterium tuberculosis* toxin-antitoxin systems: implications for pathogenesis, stress responses, and evolution. PLoS Genet 5:e1000767. https://doi.org/10.1371/journal.pgen.1000767
31. Robert X, Gouet P (2014) Deciphering key features in protein structures with the new ENDscript server. Nucleic Acids Res 42:W320–W324. https://doi.org/10.1093/nar/gku316
32. Roy A, Kucukural A, Zhang Y (2010) I-TASSER: a unified platform for automated protein structure and function prediction. Nat Protoc 5:725–38. https://doi.org/10.1038/nprot.2010.5
33. Schrödinger L (2002) The PyMOL Molecular Graphics System, Version 1.8. https://www.pymol.org/citing. Accessed 2 Jun 2017
34. Schumacher MA, Balani P, Min J, et al (2015) HipBA–promoter structures reveal the basis of heritable multidrug tolerance. Nature 524:59–64. https://doi.org/10.1038/nature14662
35. Singh J (2013) Role of D535 and H538 in endogenous toxicity of xenocin from *Xenorhabdus nematophila*. FEMS Microbiol Lett 338:147–154. https://doi.org/10.1111/1574-6968.12045

36. Singh R, Iii CEB, Boshoff HIM (2010) The three rele homologs of *Mycobacterium tuberculosis* have individual , drug-specific effects on bacterial antibiotic tolerance https://doi.org/10.1128/JB.01285-09
37. Singh R, Singh M, Arora G, et al (2013) Polyphosphate deficiency in *Mycobacterium tuberculosis* is associated with enhanced drug susceptibility and impaired growth in guinea pigs. J Bacteriol 195:2839–2851. https://doi.org/10.1128/JB.00038-13
38. Solovyev V, Salamov A (2010) Automatic annotation of microbial genomes and metagenomic sequences
39. Song S, Wood TK (2020) Toxin/antitoxin system paradigms: toxins bound to antitoxins are not likely activated by preferential antitoxin degradation. Adv. Biosyst. 4:1900290
40. Stilwell MD, Cao M, Goodrich-Blair H, Weibel DB (2018) Studying the symbiotic bacterium *Xenorhabdus nematophila* in individual, living *Steinernema carpocapsae* nematodes using microfluidic systems. https://doi.org/10.1128/mSphere.00530-17
41. Thomet M, Trautwetter A, Ermel G, Blanco C (2019) Characterization of HicAB toxin-antitoxin module of *Sinorhizobium meliloti.* BMC Microbiol 19:1–12. https://doi.org/10.1186/s12866-018-1382-6
42. Yadav M, Rathore JS (2018) TAome analysis of type-II toxin-antitoxin system from *Xenorhabdus nematophila*. Comput Biol Chem 76:293–301. https://doi.org/10.1016/j.compbiolchem.2018.07.010
43. Yamaguchi Y, Park J-H, Inouye M (2011) Toxin-Antitoxin Systems in Bacteria and Archaea. Annu Rev Genet 45:61–79. https://doi.org/10.1146/annurev-genet-110410-132412
44. Yang J, Yan R, Roy A, et al (2014) The I-TASSER Suite: protein structure and function prediction. Nat Methods 12:7–8. https://doi.org/10.1038/nmeth.3213
45. Zhang J, Zhang Y, Inouye M (2003) Characterization of the interactions within the mazEF addiction module of *Escherichia coli*. J Biol Chem 278:32300–32306. https://doi.org/10.1074/jbc.M304767200
46. Zhang Y (2008) I-TASSER server for protein 3D structure prediction. BMC Bioinformatics 9:40. https://doi.org/10.1186/1471-2105-9-40
47. Zheng C, Zhao X, Zeng T, et al (2017) Identification of four type II toxin-antitoxin systems in *Actinobacillus pleuropneumoniae*. FEMS Microbiol Lett 364:. https://doi.org/10.1093/femsle/fnx126

# Figures

Fig. 1

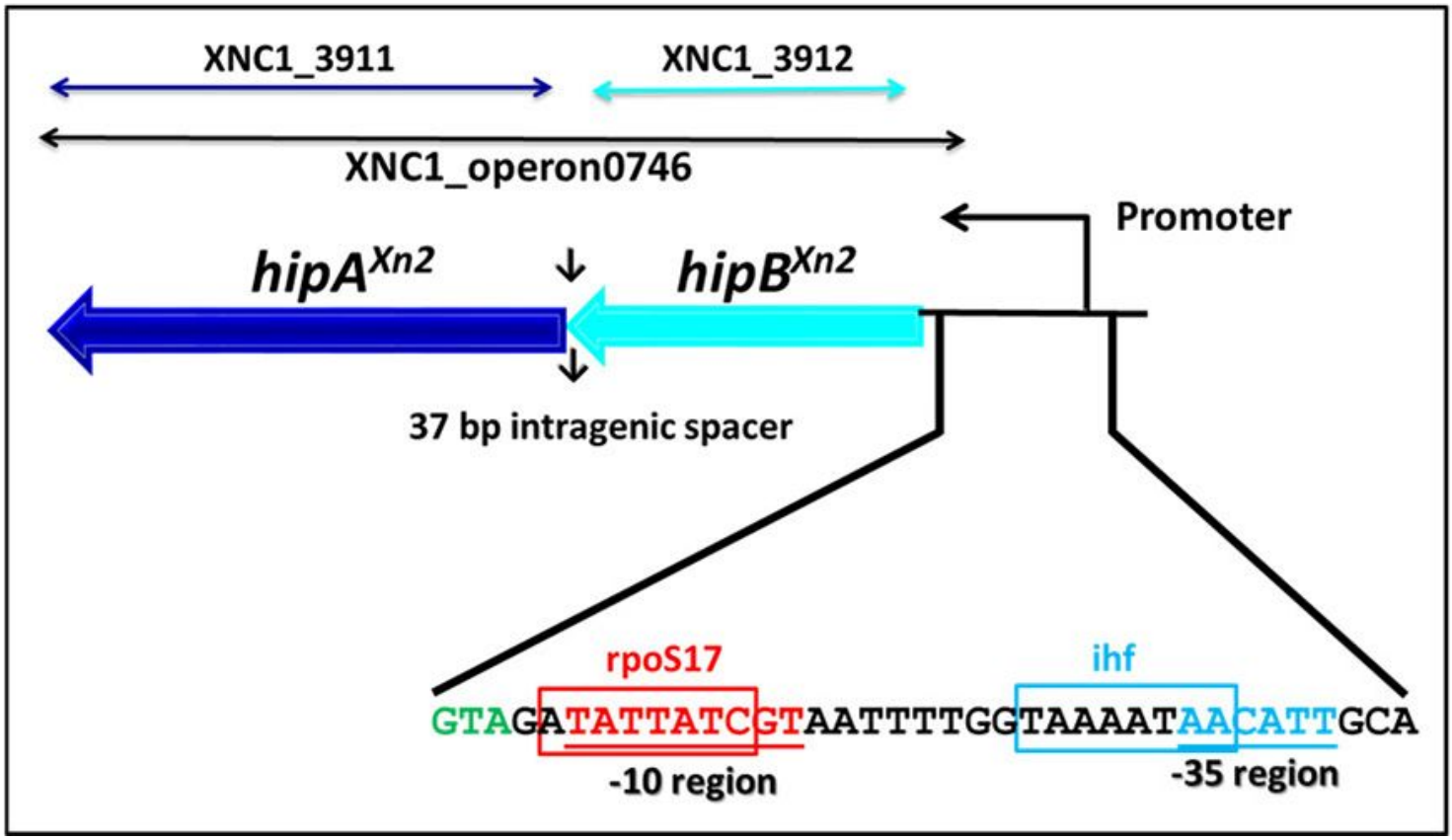


**Figure 1**

Chromosomal organization of hipBAXn2 TA system in the bacterium X. nematophila ATCC 19061, here, hipBXn2 antitoxin gene (cyan color) is located upstream to hipAXn2 toxin gene (blue color). The promoter sequence is also identified with -10 region underline in red color and -35 region underline with cyan color while rpoS17 and ihf transcription factor binding sites are indicated in red and cyan color boxes respectively

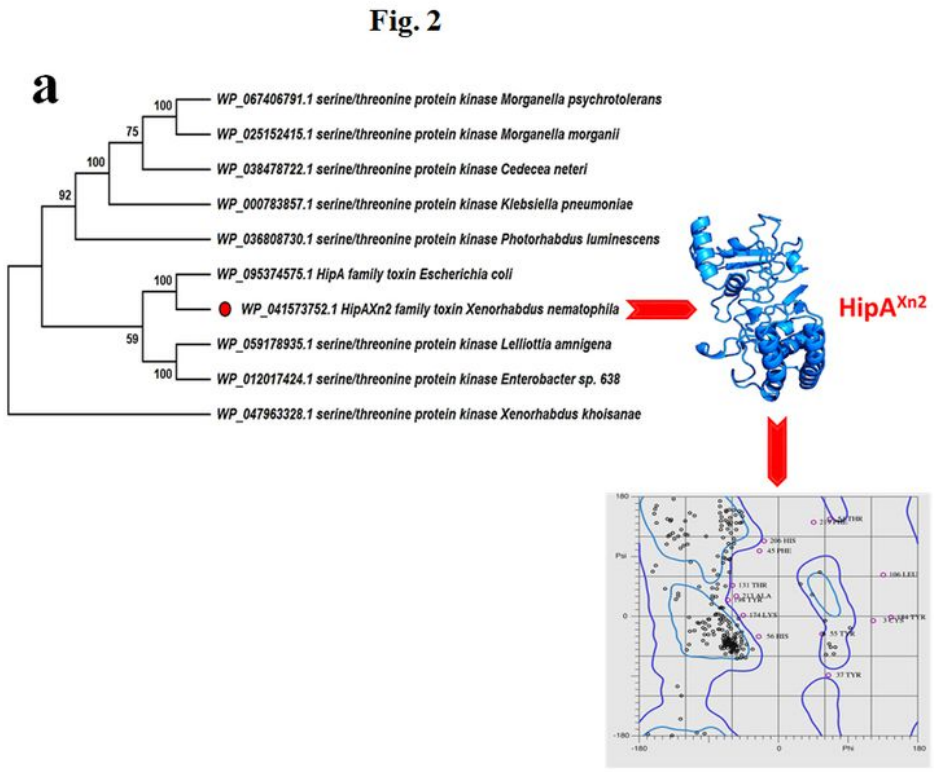


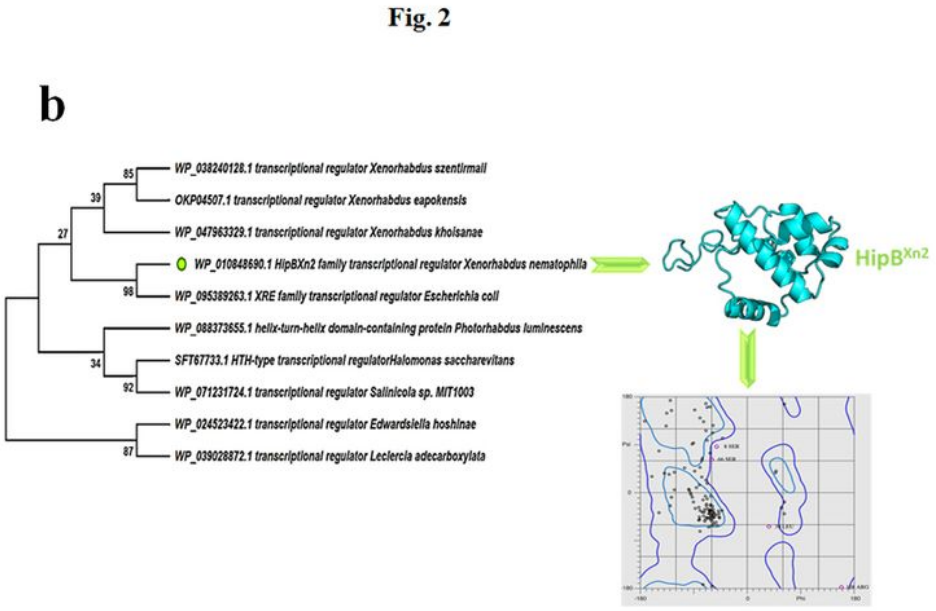


## Figure 2

Phylogenetic analysis and structural modeling of HipAXn2 toxin and HipBXn2 antitoxin from X. nematophila. a HipAXn2 toxin is indicated by a red circle with its structural model and further validated by Ramachandran plot analysis. b HipBXn2 antitoxin indicated by a green circle with its structural model and further validated by Ramachandran plot analysis

# Fig. 3

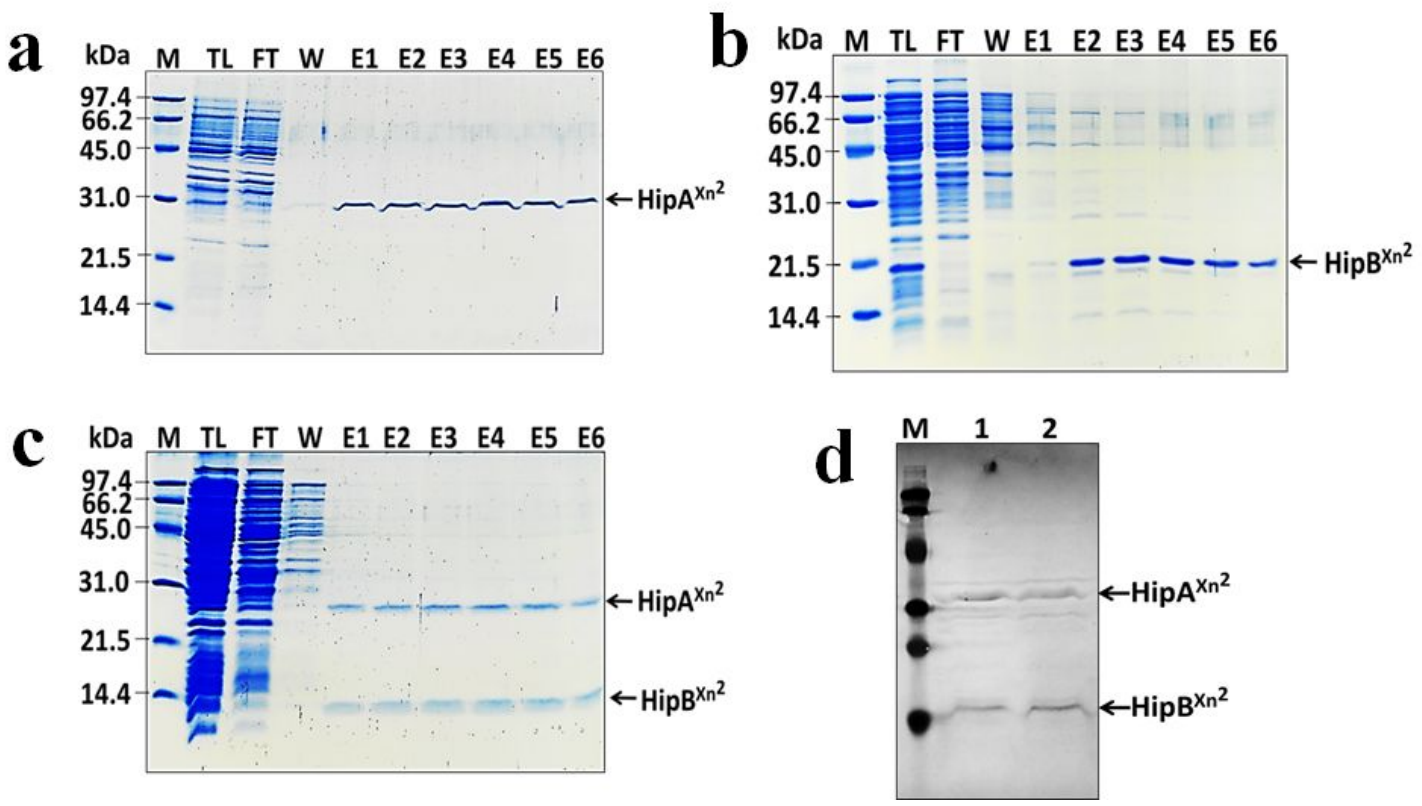


## Figure 3

Recombinant HipAXn2 toxin and HipBXn2 antitoxin on 15% SDS-PAGE. a Purification analysis of recombinant HipAXn2 toxin. b Purification analysis of recombinant HipBXn2 antitoxin. c Purification analysis of recombinant HipAXn2 toxin and HipBXn2 antitoxin proteins. Here, Lane M: Molecular weight marker, Lane TL: Total lysate, Lane FT: Flow-through, Lane W: Wash, and Lane E1-E6: Eluted fractions. d Western blot confirmation of HipAXn2 toxin and HipBXn antitoxin with anti-His monoclonal antibodies, where lane M: Molecular weight marker, lane 1 and 2: HipAXn toxin and HipBXn antitoxin

# Fig. 4

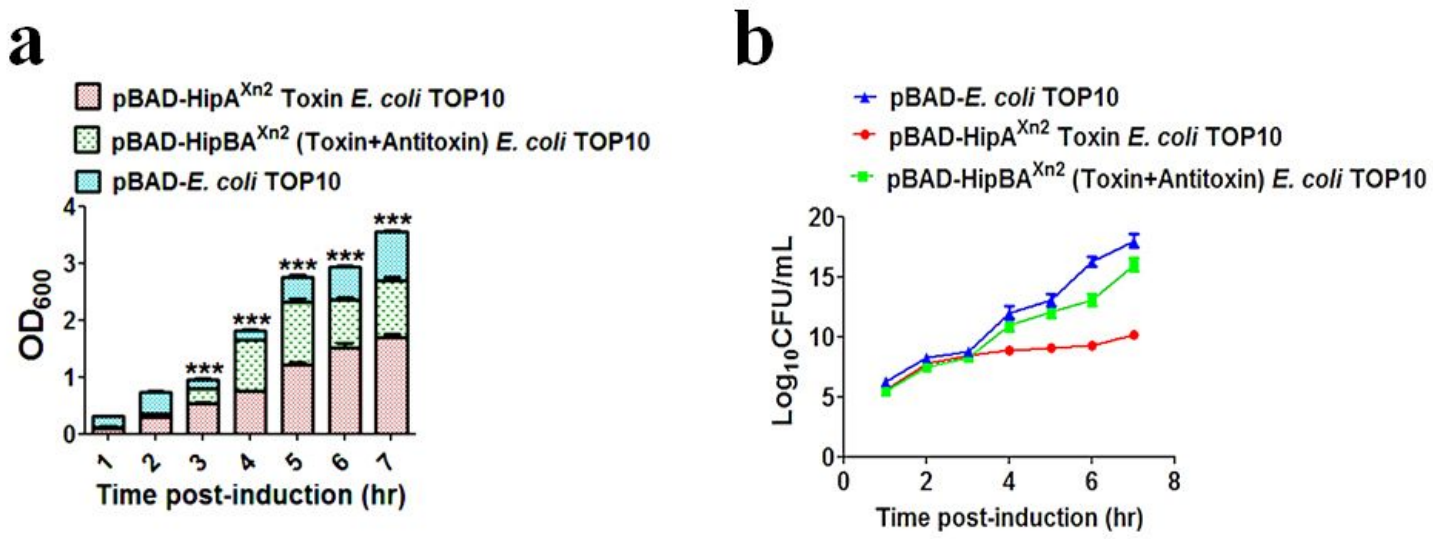


## Figure 4

Functional assessment of the hipBAXn2 TA system. a Toxicity assay in the liquid medium, here, red bars show the growth profile of cells overexpressing HipAXn2 toxin, while green bars show the growth profile of cells overexpressing both HipAXn2 toxin and HipBXn2 antitoxin simultaneously, and blue bars are used for exhibiting the growth pattern of control containing pBAD/His C empty vector in E.coli cells. Significance was tested by Two way ANOVA test, *** is $P < 0.001$, and error bars are an average of three experiments with standard deviations. b Toxicity assay on solid medium, here, red circles shows the viable cell counts (Log10CFU/mL) of E.coli cells overexpressing HipAXn2 toxin protein, green square shows the viable cell counts (Log10CFU/mL) of E.coli cells overexpressing both HipAXn2 toxin and HipBXn2 antitoxin proteins simultaneously, and blue triangles are used to exhibit the viable cell counts (Log10CFU/mL) of E. coli cells having pBAD/HisC empty vector. Error bars indicate mean ±SD from three independent experiments

# Fig. 5

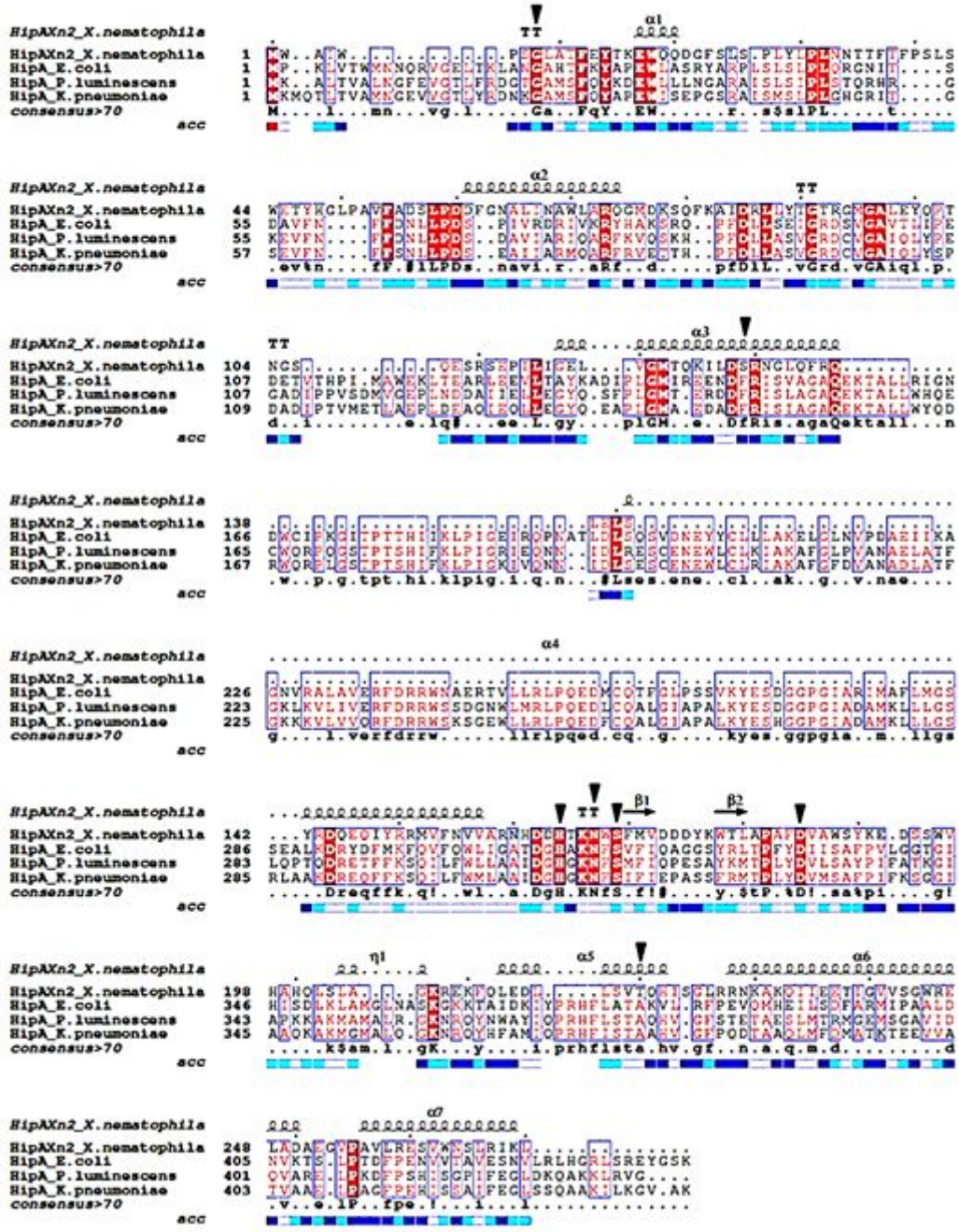


## Figure 5

Multiple sequence alignment of HipAXn2 toxin. This toxin was aligned with other HipA toxins from Photorhabdus luminescens, Klebsiella pneumoniae, and Escherichia coli by MAFFT (Katoh and Standley 2013) and represented with ESPript 3.0. (Robert and Gouet 2014). Identical and conserved residues are illustrated by a red background and the active site residues used in site-directed mutagenesis are shown by black arrows.

Fig. 6

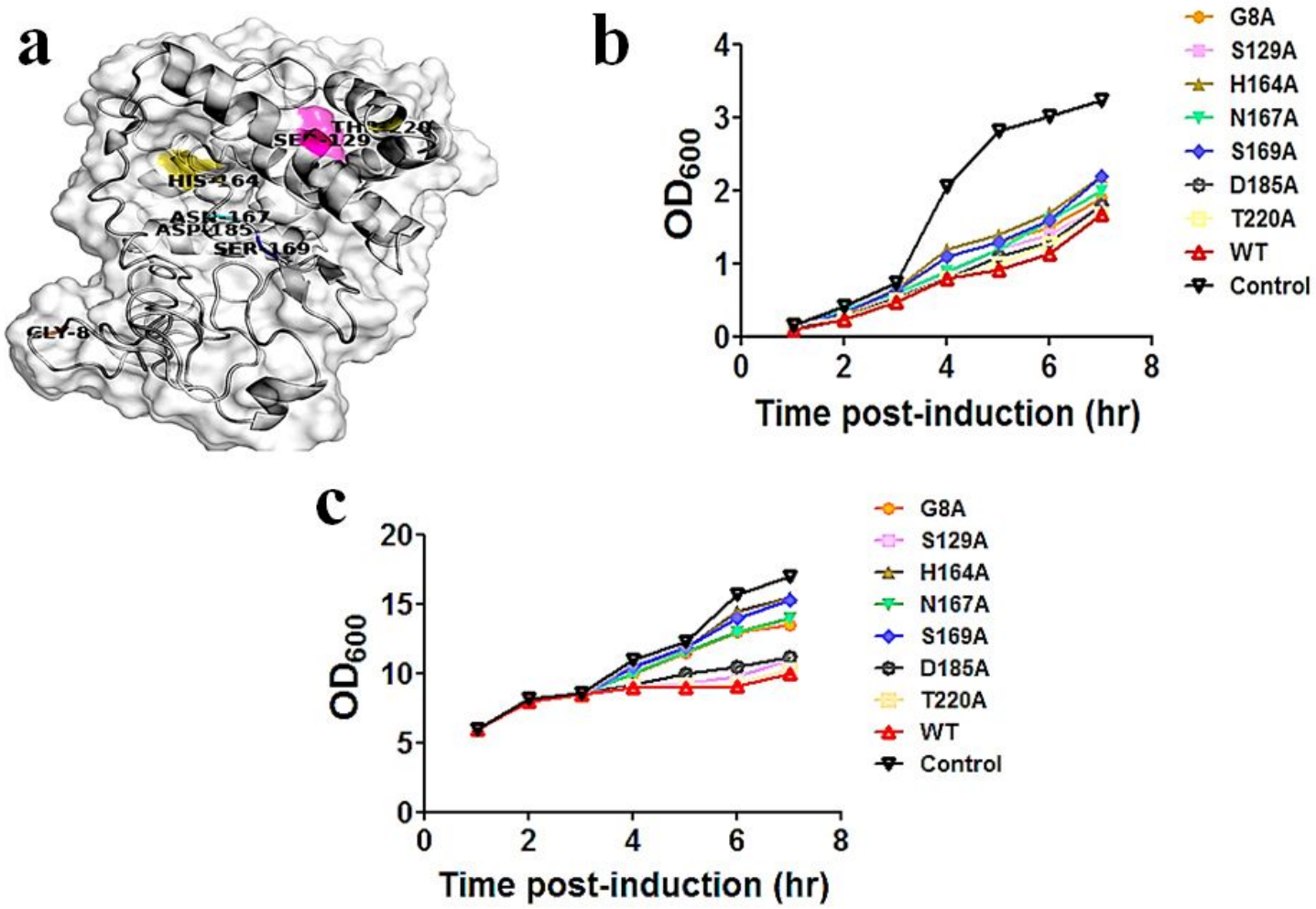


## Figure 6

Site-Directed Mutagenesis analysis in the active site of HipAXn2 toxin. A The active site residues for the mutation in HipAXn2 toxin, cartoon structure on the transparent surface of this protein is shown and mutated residues are labeled. b Growth pattern of hipAXn2 toxin and its mutants, here, black triangle is Control and wild type (WT) is red triangle while mutants Gly-8, Ser-129, His-164, Asn-167, Ser-169, Asp-185, and Thr-220 are depicted with an orange circle, violet square, brown triangle, green square, blue square, grey circle, and yellow square respectively, c Graph between the number of viable E. coli cells (Log10CFU/mL) overexpressing HipAXn2 toxin and its mutants against time post-induction, here, control strain is shown with the black triangle (Control), wild type (WT) is shown with a red triangle and while mutants G8A, S129A, H164A, N167A, S169A, D185A, and T220A are shown with an orange circle, violet square, brown triangle, green square, blue square, grey circle, and yellow square respectively

# Fig. 7

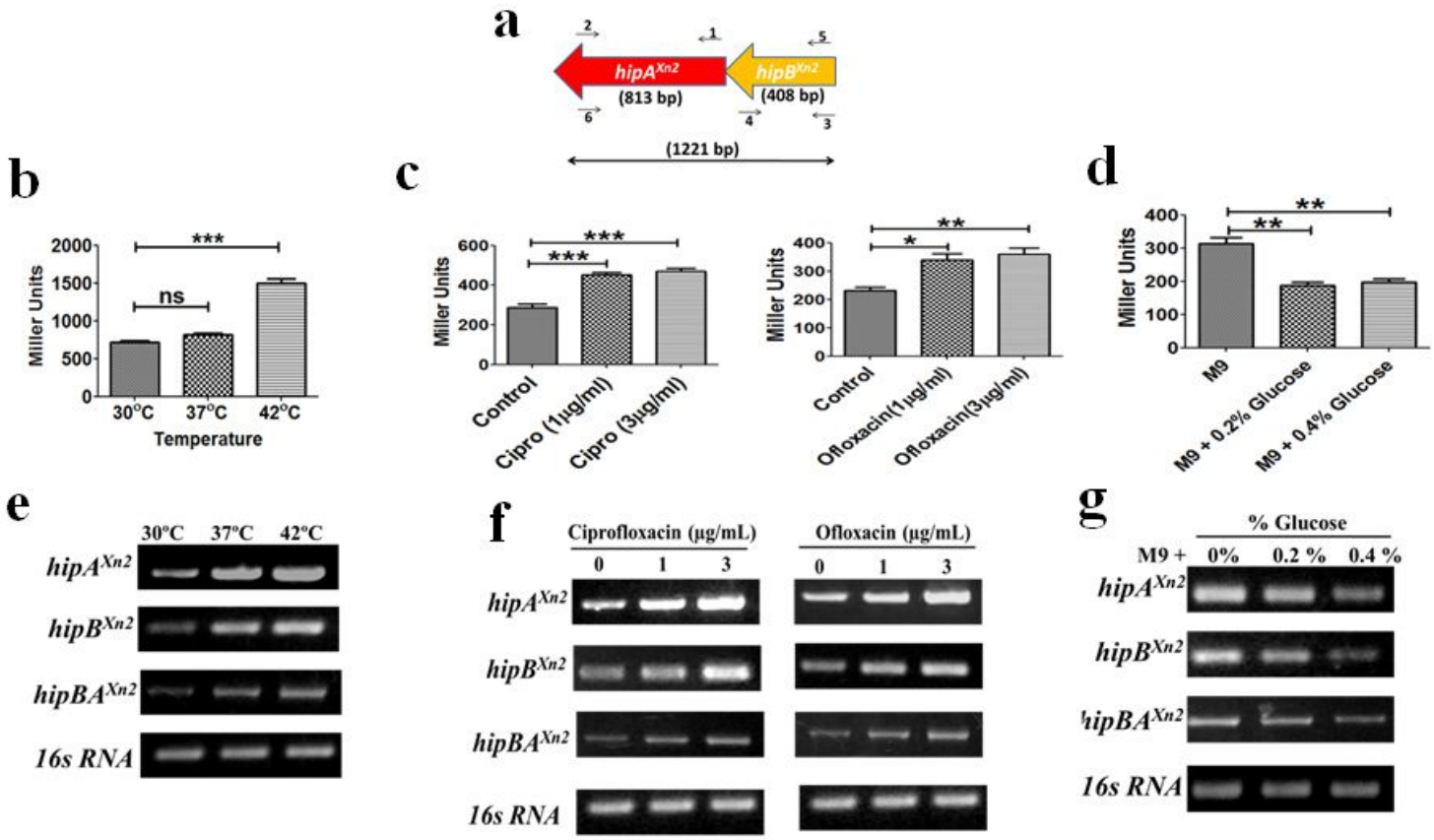


## Figure 7

Transcriptional regulatory analysis of the hipBAXn2 TA system under different stress conditions. a The diagrammatic representation of TA genes and primers used in the RT-PCR expression analysis; genes sizes are in bp and arrow numbers represent the number of primers as described in Table S2. lacZ assays for hipBAXn2 TA promoter under b elevated temperature stress condition, c ciprofloxacin and ofloxacin antibiotics stress condition, d nutritional starvation stress condition; β-galactosidase activity in Miller Units (MU), here, ***P<0.0001, **P=0.002, **P<0.05 and ns: not significant. Error bars are the mean ± SEM from three independent experiments and statistical analysis was done by one way ANOVA while comparison was performed by Tukey's Multiple Comparison Test. Reverse transcriptase-polymerase chain reaction expression analysis of hipBAXn2 TA system under e elevated temperature stress condition, f ciprofloxacin and ofloxacin antibiotics stress condition, g nutritional starvation stress condition

# Fig. 8

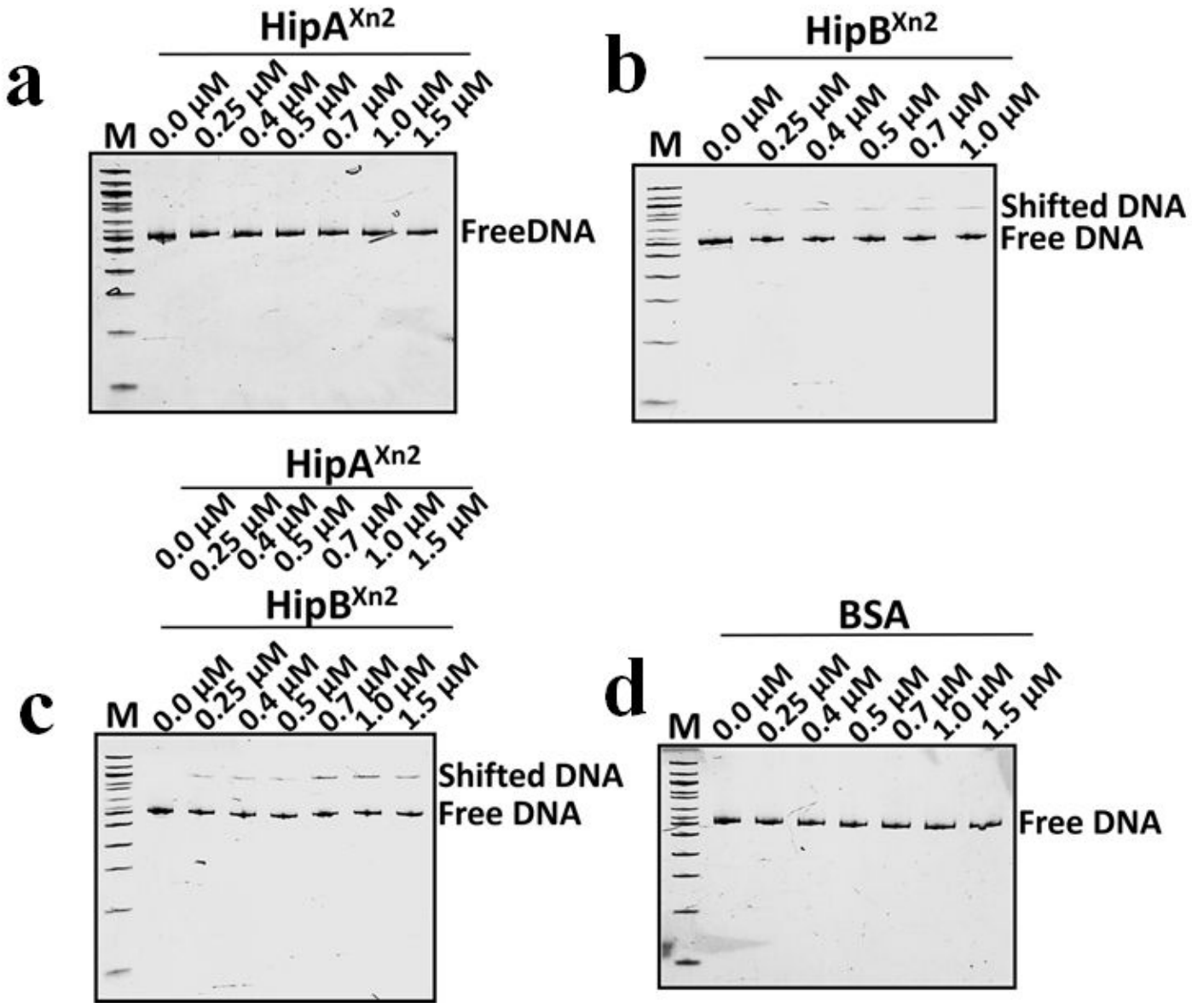


**Figure 8**

Electrophoretic mobility shift assay of the hipBAXn2 TA system. a No gel shift was observed for the hipBAXn2 TA promoter interacting with recombinant HipAXn2 toxin. b The faint gel shift was for the hipBAXn2 TA promoter interacting with recombinant HipBXn antitoxin. C Gel shift was enhanced when the hipBAXn2 TA promoter interacts with both recombinant HipBXn antitoxin and HipAXn toxin together and d No gel shift was observed while hipBAXn2 TA promoter interacts with BSA protein. DNA-binding characteristic of purified recombinant HipAXn2 toxin and HipBXn2 antitoxin was confirmed by incubating 200 ng of hipBAXn2 promoter with the concentration gradient of recombinant proteins in µM as indicated in this figure.

Fig. 9

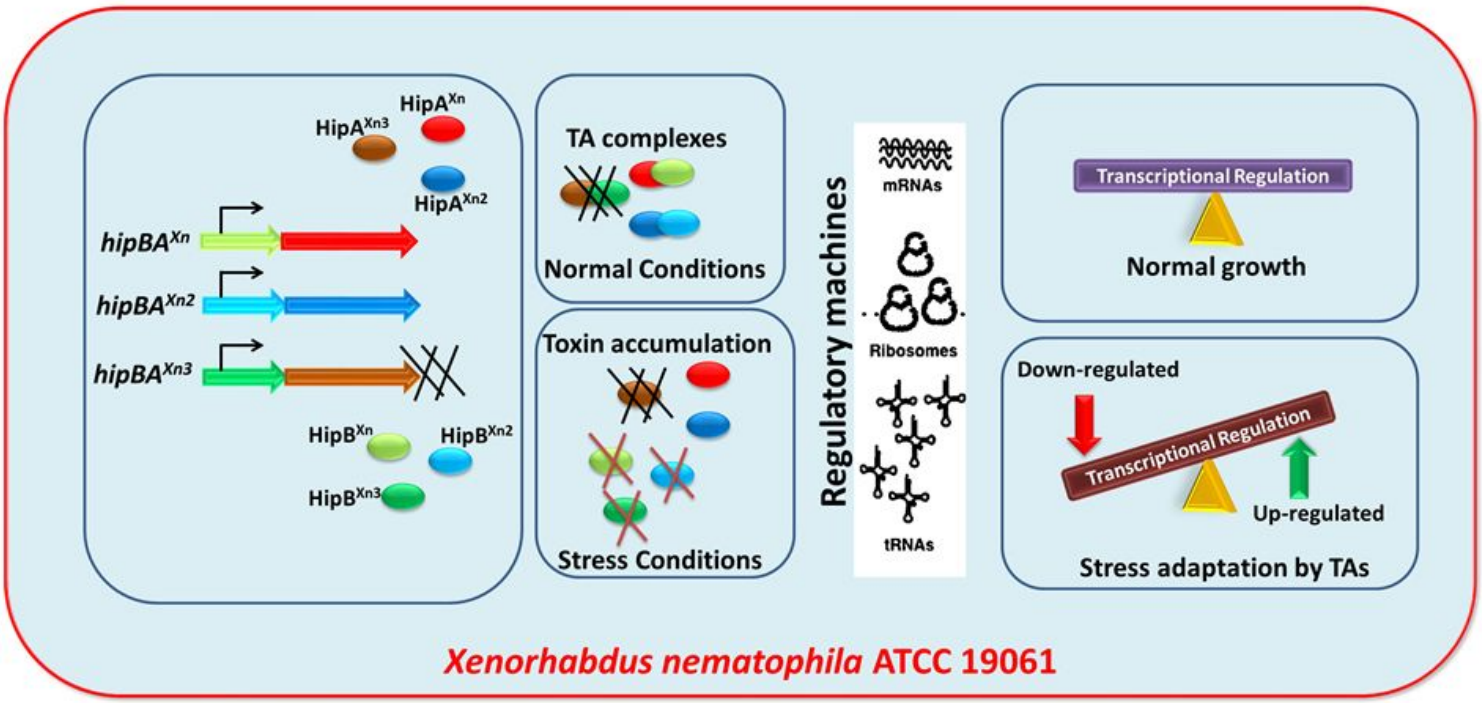


**Figure 9**

A schematic model proposed for the transcriptional regulation of hipBAXn, hipBAXn2, and hipBAXn3 TA systems in X. nematophila. In normal growth conditions, these TA complexes work as a repressor and negatively regulate the transcription. In stress conditions, these antitoxins are selectively degraded by cellular proteases and the cognate toxins are free to inhibit translation by affecting transcriptional machinery. Thus, these TAs are involved in bacterial physiology by reprogramming cells to reduce cellular growth with up and down regulating necessary genes to facilitate cell survival in the different stresses.

## Supplementary Files

This is a list of supplementary files associated with this preprint. Click to download.

- Supplementarymaterial.docx